Cancer Research

HDAC Inhibitor Panobinostat Engages Host Innate Immune Defenses to Promote the Tumoricidal Effects of Trastuzumab in HER2$^+$ Tumors

Mikolaj Medon[1,2], Eva Vidacs[1], Stephin J Vervoort[1], Jason Li[3], Misty R. Jenkins[4,5], Kelly M. Ramsbottom[4], Joseph A. Trapani[4,5], Mark J. Smyth[6], Phillip K. Darcy[4,5], Peter W. Atadja[7], Michael A. Henderson[2], Ricky W. Johnstone[1,5], and Nicole M. Haynes[1,5]

Abstract

Histone deacetylase inhibitors (HDACi) may engage host immunity as one basis for their antitumor effects. Herein, we demonstrate an application of this concept using the HDACi panobinostat to augment the antitumor efficacy of trastuzumab (anti-HER2) therapy, through both tumor cell autonomous and nonautonomous mechanisms. In HER2$^+$ tumors that are inherently sensitive to the cytostatic effects of trastuzumab, cotreatment with panobinostat abrogated AKT signaling and triggered tumor regression in mice that lacked innate and/or adaptive immune effector cells. However, the cooperative ability of panobinostat and trastuzumab to harness host anticancer immune defenses was essential for their curative activity in trastuzumab-refractory HER2$^+$ tumors. In trastuzumab-resistant HER2$^+$ AU565^{PV} xenografts and BT474 tumors expressing constitutively active AKT, panobinostat enhanced the antibody-dependent cell-mediated cytotoxicity function of trastuzumab. IFNγ–mediated, CXCR3-dependent increases in tumor-associated NK cells underpinned the combined curative activity of panobinostat and trastuzumab in these tumors. These data highlight the immune-enhancing effects of panobinostat and provide compelling evidence that this HDACi can license trastuzumab to evoke NK-cell–mediated responses capable of eradicating trastuzumab-refractory HER2$^+$ tumors. *Cancer Res; 77(10); 2594–606. ©2017 AACR.*

Introduction

Approximately 20% to 30% of breast cancers overexpress the HER2/neu oncogene–encoding HER2 (1). Active dimers of HER2 with other family members promote tumorigenesis by enhancing tumor cell growth and survival (2). Targeted blockade of HER2 signaling with the humanized antibody (Ab) trastuzumab (Herceptin) has substantially improved prognosis for HER2-positive breast cancer patients (3). By binding HER2, trastuzumab can induce cell-cycle arrest and/or inhibit DNA repair (3). It can also trigger immune-mediated tumor cell death through antibody-dependent cell-mediated cytotoxicity (ADCC) and may evoke therapeutically beneficial adaptive immune responses (4). However, despite these pleiotropic actions of trastuzumab, less than 35% of HER2$^+$ breast cancers demonstrate initial response to trastuzumab and of those patients with metastatic disease who initially respond to anti-HER2-based chemotherapy, 70% relapse within a year of treatment initiation (5).

Histone deacetylase inhibitors (HDACi) are anticancer drugs that can mediate a diverse array of biological responses, including induction of apoptosis and cell-cycle arrest, inhibition of angiogenesis, and promotion of tumor cell differentiation (6). From an immunological perspective, HDACi can modulate the effector functions of activated immune cells and promote the efficacy of immunotherapeutic strategies in established solid tumors (7, 8). HDACi may engage anticancer immune responses by directly altering tumor cell immunogenicity, and have the potential to rescue the functional activity of exhausted CD8$^+$ T cells (9, 10). By modulating the activity and accumulation of regulatory immune cells in tumors, HDACi may also influence the immunosuppressive nature of the tumor microenvironment (10).

HDACi have been shown to potentiate the antitumor effects of trastuzumab and lapatinib against trastuzumab-sensitive, HER2$^+$ tumor cell lines *in vitro* (11–14). Such findings have established grounds for testing HDACi in combination with trastuzumab and chemotherapy in early-phase clinical

[1]Cancer Therapeutics Program, Peter MacCallum Cancer Centre, Victorian Comprehensive Cancer Centre (VCCC), Melbourne, Victoria, Australia. [2]Division of Surgical Oncology, Peter MacCallum Cancer Centre, VCCC, Melbourne, Victoria, Australia. [3]Bioinformatics Consulting Core Facility, Cancer Research Division, Peter MacCallum Cancer Centre, VCCC, Melbourne, Victoria, Australia. [4]Cancer Immunology Research Program, Peter MacCallum Cancer Centre, VCCC, Melbourne, Victoria, Australia. [5]Sir Peter MacCallum Department of Oncology, The University of Melbourne, Parkville, Victoria, Australia. [6]Immunology in Cancer and Infection Laboratory, QIMR Berghofer Medical Research Institute, Herston, Queensland, Australia. [7]China Novartis, Institute for Biomedical Research, Shanghai, China.

Note: Supplementary data for this article are available at Cancer Research Online (http://cancerres.aacrjournals.org/).

N.M. Haynes and R.W. Johnstone contributed equally and are co-senior authors of this article.

Corresponding Author: Nicole M. Haynes, Peter MacCallum Cancer Centre, Victorian Comprehensive Cancer Centre, 305 Grattan Street, Melbourne, Victoria 3000, Australia. Phone: 613-8559-7127; Fax: 613-8559-5039; E-mail: nicole.haynes@petermac.org

doi: 10.1158/0008-5472.CAN-16-2247

trials with promising activity (15, 16). Here, we examine the combined anticancer activity and mechanisms of synergy between trastuzumab and the HDACi panobinostat in models of trastuzumab-sensitive and -refractory HER2$^+$ cancer. We demonstrate the novel curative capacity of this anti–HER2-based combination therapy and its ability to engage host innate immune cells and effector molecules to evoke durable therapeutic responses against trastuzumab-refractory HER2$^+$ tumors.

Materials and Methods

Mice

Six- to 8-week-old SCID mice were obtained from the Australian Resources Centre (Perth, Western Australia). NOD/SCID IL2Rγ$^{-/-}$ (NSG) and BALB/c MMTV-Her2/*neu* transgenic mice were bred in-house and genotyped at the Peter MacCallum Cancer Centre (PMCC; ref. 17). All animal experiments were performed in accordance with institutional guidelines of the PMCC.

Cell lines

The AU565 and BT474 cell lines were purchased from the ATCC (2009; both lines were last authenticated in July 2015). BT474 tumor cells were maintained in RPMI1640, 10% FBS, 2 mmol/L L-glutamine, 0.1 mmol/L nonessential amino acids, 1 mmol/L sodium pyruvate, and 0.1 mmol/L HEPES. AU565 tumor cells were maintained in RPMI-1640, 10% FBS, 2 mmol/L L-glutamine and 0.1 mmol/L HEPES. Through multiple passages of the AU565 tumor line, we derived a variant (AU565^{pv}) that could be xenografted into NSG and SCID mice. MSCV-GFP/Bcl2 and MSCV-GFP/AKT (myristolated AKT (MyrAKT)) were transduced into the BT474 and/or AU565^{pv} cells as described previously (18–20). The rat HER2$^+$ murine H2N100 and H2N113 mammary carcinoma cell lines (derived from MMTV Her2/*neu* transgenic mice; ref. 21) and YAC-1 cell line were cultured in RPMI1640, 10% FBS, 2 mmol/L L-glutamine and 0.1 mmol/L HEPES. All cell lines tested negative for *Mycoplasma* contamination by PCR.

Drugs and reagents

Trastuzumab (Herceptin, Roche) was obtained through the PMCC Pharmacy. Panobinostat was provided by Novartis Pharmaceutical Inc. (Shanghai, China). For *in vitro* studies, panobinostat was dissolved in dimethyl sulfoxide (Calbiochem) at a 10 mmol/L stock solution. For *in vivo* studies, panobinostat was dissolved by sonication in 5% dextrose to make a 1 mg/mL stock solution. Depletion antibodies to asialoGM1 [natural killer (NK) cells; ≥90% depletion efficiency; Wako Pure Chemical] and CD8β (53.5.8; ≥85% depletion efficiency; BioXCell) were prepared as described previously (22). Blocking or neutralizing antibodies to CD16/CD32 Fc receptors (2.4G2), IFNγ (XMG1.2), CXCR3 (CD183) and CD11b were prepared as described previously (antibodies from BioXCell; ref. 22).

Cell proliferation and death assays

Proliferation assay. Tumor cells (10^3) were treated with 0–10 μg/mL trastuzumab or 10 μg/mL CIg for 5 days. For the last 16 hours, 0.5 μCi tritiated thymidine was added. Levels of tritiated thymidine incorporation were measured using a β-counter (PerkinElmer). Six-replicate wells/group analyzed. Cell death assays: 10^4 tumors cells were treated with: (i) 1–200 nmol/L panobinostat or corresponding DMSO concentrations for 24–48 hours or (ii) 1 μg/mL trastuzumab or control human IgG1 (Enzo Life Sciences) for 96 hours before addition of 20 nmol/L panobinostat or DMSO for 24 hours. Vehicle- and drug-treated cells were stained with Annexin-V-FITC (BD Pharmingen)/propidium iodine (PI) and analyzed on a LSRII analyzer (BD Biosciences). Two replicate wells/group were analyzed. A 4-hour ^{51}Cr release assay (as described; ref. 22) was used to assess the effects of panobinostat on NK-cell cytotoxicity and tumor cell sensitivity to NK-cell killing. IL2–activated mouse NK cells were: (i) cultured in 10 nmol/L panobinostat or DMSO for 20 hours before being cocultured with ^{51}Cr-labeled target cells or (ii) cultured with ^{51}Cr-labeled targets that had been pretreated for 20 hours with 5–50 nmol/L panobinostat.

Western blot analysis

Immunoblots were performed on whole-cell lysates (19). Tumor cell cultures were treated as outlined above in the presence of 10 μmol/L qVD (InSolution Q-VD-OPh; Calbiochem). Protein/sample was resolved on 10% SDS-PAGE gels. Antibodies against human HER2 (tyr1248; Cell Signaling Technology), AKT (Cell Signaling Technology), pAKT (Ser473; 193H12; Cell Signaling Technology), Bcl-2 (Cell Signaling Technology), and β-Actin (Sigma-Aldrich) were used as probes that were detected using horseradish peroxidase–conjugated secondary Abs (DAKO) and enhanced chemiluminescence (ECL, Amersham; Lumilight, Roche).

Therapy of transplanted tumors

BT474 (3×10^6) or AU565^{pv} (1.5×10^6) tumor cells were orthotopically injected into the fourth mammary fat pad of SCID or NSG mice. 0.72 mg estrogen pellets (Innovative Research of America) were implanted subcutaneously at the time of BT474 tumor inoculation. In some experiments, tumor-free NSG mice were reconstituted with 1.5×10^6 mouse splenic NK cells, twice enriched (90%–95% purity) using an NK Cell Isolation Kit (StemCell Technologies). Seven days after NK-cell reconstitution, AU565^{pv} tumor cells were orthotopically injected. A total of 5×10^5 H2N100 or H2N113 tumor cells were injected subcutaneously into MMTV-HER2/*neu* transgenic mice.

Tumor growth was monitored every 2 to 3 days and represented as tumor area. Drug treatment commenced when tumors reached 25 mm^2. Xenograft models: Mice were treated intraperitoneally with vehicle (PBS + 5% glucose water), panobinostat (15 mg/kg on days 1–5 and 8–12), trastuzumab (10 mg/kg on days 1, 4, 8, 11), or panobinostat plus trastuzumab.

Syngeneic models. α-rHER2 Abs (7.16.4; 100 μg on days 1, 4, 8, 11) were administered with panobinostat (15 mg/kg) or doxorubicin. Doxorubicin was injected intravenously (2 mg/kg) or intratumoral (i.t.; 50 μL of a 2 mmol/L stock) on days 0 and 7. Isotype control immunogobulins (CIg, 100–300 μg; Bio X cell), depleting (α-asialoGM1, 100 μg; α-CD8β, 100μg), neutralizing (α-CD11b, 300 μg; α-IFNγ, 200 μg) and blocking (α-CD16/CD32 [2.4G2], 100 μg; α-CXCR3, 150 μg) antibodies were administered intraperitoneally on days –1, 0, 3, 6, 9, 12, 15, 18 relative to therapy.

All mice were sacrificed when tumors reached 100–150 mm^2. Mice cleared of tumor were monitored out to days 80–100 posttumor clearance.

Ex vivo analysis of tumor-infiltrating leukocytes

Analysis of tumor-infiltrating leukocytes was conducted on days 1, 2, 6, 9 posttherapy initiation. Dissected tumors were mechanically and enzymatically dissociated in collagenase IV (Worthington Biochemical Corporation). Cell suspensions were stained for the pan-leukocyte marker CD45.2 (eBioscience). Tumor-associated CD49b$^+$ NK cells (DX5) were characterized for the differentiation markers CD27 (LG.7F9) and CD11b (M1/70), activation receptor CD69 (H1.2F3) and CD16/CD32 Fc-receptors (93). Myeloid cell populations were staining for Ly-6C (HK1.4), CD11b and Ly-6G (all antibodies from eBioscience). Cell viability determined using DAPI (4′,6-diamido-2-phenlindole; Invitrogen). Cells were analyzed on a LSRII analyzer (BD Biosciences). All tumor samples were analyzed using the same viable cell (DAPI$^-$) collection gate cutoff to eliminate any biases relating to therapy-induced differences in tumor size/group.

Flow cytometric analysis of *in vitro*–enriched mouse and human NK cells

Mouse splenic NK cells were enriched using a NK cell isolation kit (80%–85% purity; StemCell Technologies) and cultured for 5-days in 1,000 U/mL IL2. Human NK cells were isolated from peripheral blood of healthy donors using a MACS NK cell isolation kit and autoMACs separator (MACS; Miltenyi Biotec) and cultured for 1 to 3 days in 25 U/mL IL2. NK cells were maintained in RPMI-1640 supplemented, 10% FBS, 2 mmol/L L-glutamine, 10 mmol/L HEPES, 1 mmol/L sodium pyruvate, 100 μmol/L nonessential amino acids, 50 μmol/L 2-ME. NK cells were treated with 2.5–20 nmol/L panobinostat for 20 hours before being stained with antibodies to mouse CD49b, CD27, CD11b, CD69, and CD16/CD32 (BD Bioscience) or human CD56, CD16 and CD69 (BD Biosciences) as described above and analyzed on a LSRII analyzer.

RNA sequencing

RNA was extracted from whole AU565^{pv} tumors, harvested from SCID mice 2 days posttreatment initiation with vehicle, panobinostat, trastuzumab or panobinostat plus trastuzumab (as outlined above) using an RNeasy Plus Mini Kit (Qiagen). RNA was sequenced on the Illumina HighSeq 2000. Sequenced data were processed using Seqliner v0.2.0 (seqliner.org) RNA-seq analysis pipeline. Short read data were first aligned using TopHat/bowtie2 (23) to the human reference genome GRCh37.p12. All unmapped reads were subsequently aligned to the mouse reference genome GRCm38/mm10. Read counting was performed with HTSeq-Count from HTSeq (24) using transcript annotation from Degust Version 0.20 (Victorian Bioinformatics Consortium, Monash University and VLSCI's Life Sciences Computation Centre). The Voom-LIMMA workflow was used to normalize data and compute differential gene expression (25). All processed and raw RNAseq data files were deposited into the Gene Expression Omnibus/Sequencing Read Archive.

Statistical analysis

Statistical differences between groups were analyzed with an unpaired Student *t* test (*in vitro* experiments) or a Mann–Whitney *U* or Log-rank (Mantel–Cox) test (*in vivo* experiments) using GraphPad Prism (GraphPad Software).

Results

Cotreatment of panobinostat and trastuzumab can eradicate established trastuzumab-sensitive HER2$^+$ breast tumors

The combinatorial effects of panobinostat and trastuzumab were examined *in vitro* against the trastuzumab-sensitive HER2$^+$ breast tumor line BT474. Trastuzumab suppressed the proliferation of BT474 tumor cells in a dose-dependent manner (Fig. 1A) and increased their sensitivity to panobinostat-induced cell death as determined by Annexin-V/PI staining (Fig. 1B).

BT474 tumor cells were grown orthotopically in the mammary fat pad of NSG mice that lack T, B, and NK cells and have a dysfunctional myeloid compartment (26). Single-agent panobinostat or trastuzumab therapy suppressed tumor growth and prolonged survival of tumor-bearing mice by 20 to 30 days relative to the vehicle treated group (Fig. 1C). Complete tumor clearance was achieved in mice treated with the combination of panobinostat and trastuzumab (Fig. 1C). Similar responses to panobinostat and trastuzumab treatment, alone and in combination were observed in SCID mice (with a competent innate immune system) orthotopically transplanted with BT474 tumors (Fig. 1D). SCID mice depleted of NK cells could also support the curative activity of the combination therapy (Fig. 1E). The combined ability of panobinostat and trastuzumab to induce antitumor responses, independent of innate and adaptive immune cells suggests that direct induction of apoptosis is sufficient to mediate the curative effects of the combination therapy in trastuzumab-sensitive HER2$^+$ tumors.

The combined therapeutic activity of panobinostat and trastuzumab was also examined in MMTV-HER2/*neu* transgenic mice bearing subcutaneously implanted H2N tumors. These tumor lines express oncogenic rat HER2 (rHER2) and are sensitive to the cytostatic and cytotoxic effects of anti-HER2 therapy (21). *In vitro* treatment of H2N100 tumor cells with the anti-rHER2 mAb, 7.16.4 increased their sensitivity to the apoptotic effects of panobinostat (Fig. 2A). Cotreatment of MMTV-HER2/*neu* transgenic mice with panobinostat and 7.16.4 was significantly more effective at controlling H2N100 tumor growth than either single agent alone (Fig. 2B). Depletion of CD8$^+$ T or NK cells did not compromise the antitumor effects of the combination therapy against H2N100 tumors (Fig. 2C); reinforcing the dominant contribution of tumor-intrinsic antiproliferative and apoptotic mechanisms to the combined tumor growth inhibitory effects of panobinostat and anti-HER2 therapy in HER2$^+$ tumors that are sensitive to the cytostatic effects of anti-HER2 therapy.

Cotreatment with panobinostat and trastuzumab can eradicate established trastuzumab-resistant HER2$^+$ xenografts

We next examined the combined therapeutic activity of panobinostat and trastuzumab in HER2$^+$ xenografts that are inherently resistant to the cytostatic effects of trastuzumab. The HER2$^+$ AU565^{pv} tumor line (confirmed to express similar levels of HER2 as the BT474 tumor line and was resistant to the antiproliferative effects of trastuzumab *in vitro* (Supplementary Fig. S1 and Fig. 3A) was modestly sensitive to the apoptotic effects of panobinostat. Addition of trastuzumab did not increase panobinostat-induced cell death (Fig. 3B).

In NSG mice bearing established AU565^{pv} tumors, trastuzumab treatment did not inhibit tumor growth and the administration of panobinostat, alone or in combination with

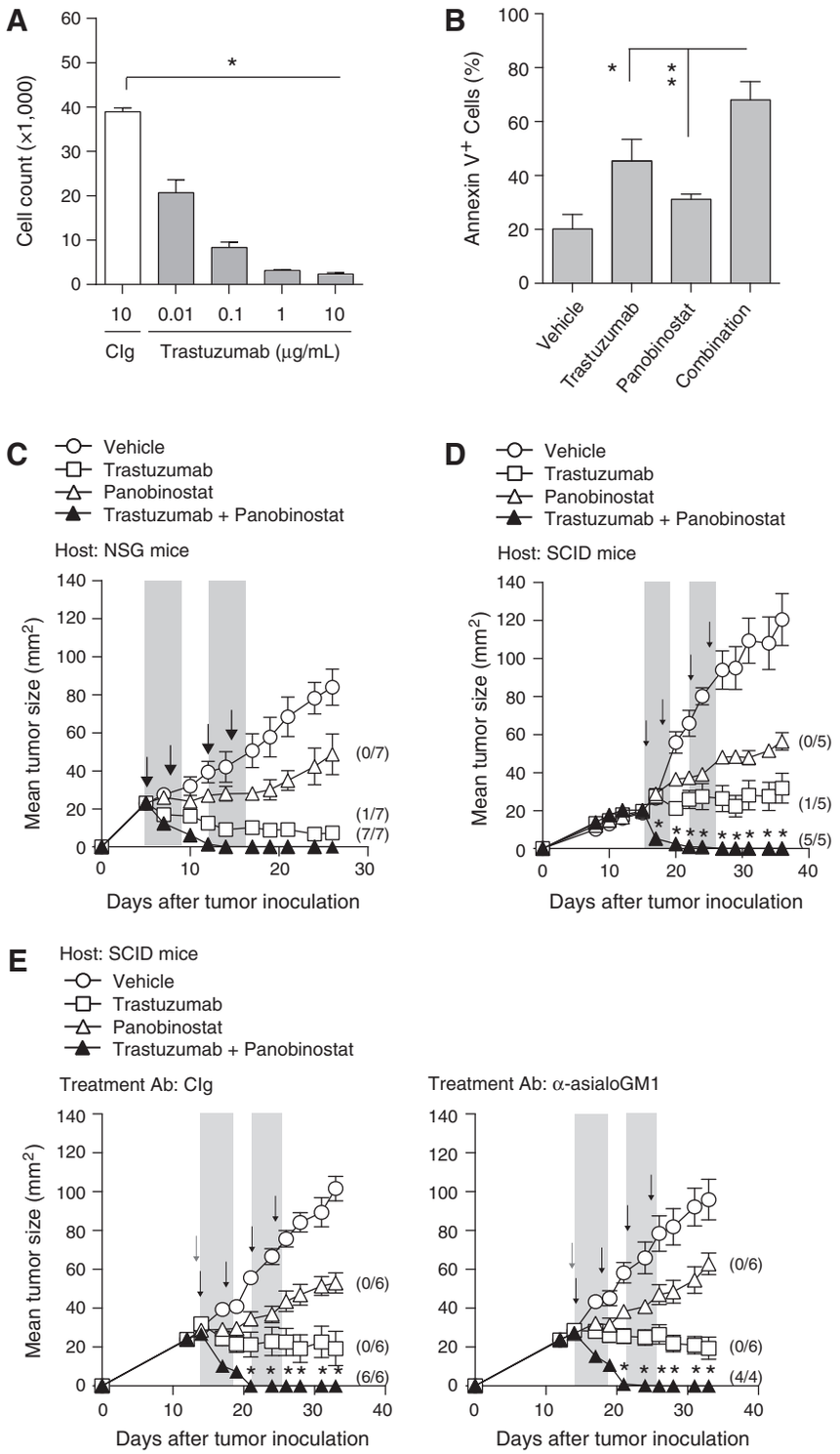

Figure 1.

Cooperative effects of trastuzumab and panobinostat against BT474 tumors. **A,** Antiproliferative effects of trastuzumab on BT474 tumor cells. Statistical differences, *, $P < 0.002$. **B,** Drug-induced BT474 tumor cell death as measured by flow cytometric analysis of Annexin-V/PI staining. Mean tumor cell death ± SEM of three independent experiments shown. Statistical differences, *, $P < 0.02$; **, $P < 0.007$. **C–E,** BT474 tumor-bearing NSG (**C**) or SCID mice (**D** and **E**) were treated as indicated. Black arrows, treatment with trastuzumab. Solid gray bars, periods of HDACi treatment. Gray arrows, the start of antibody treatment. Mean tumor size ± SEM shown ($n = 5$–7/group). Results are representative of two-independent experiments. Statistical differences, *, $P < 0.008$ (**D**); *, $P < 0.002$ (**E**), compared with single-agent treatment and control-treated groups. Parentheses indicate fraction of tumor-free mice.

trastuzumab, resulted in only a modest delay in tumor growth (Fig. 3C). In SCID mice a strikingly different antitumor effect of trastuzumab and panobinostat was observed (Fig. 3D). As single agents, both were more effective at slowing AU565^{pv} tumor growth compared with that seen in NSG mice, but when used in combination, trastuzumab and panobinostat evoked complete regression of the AU565^{pv} tumors in all mice (Fig. 3D). These data suggest that cotreatment with trastuzumab and panobinostat can

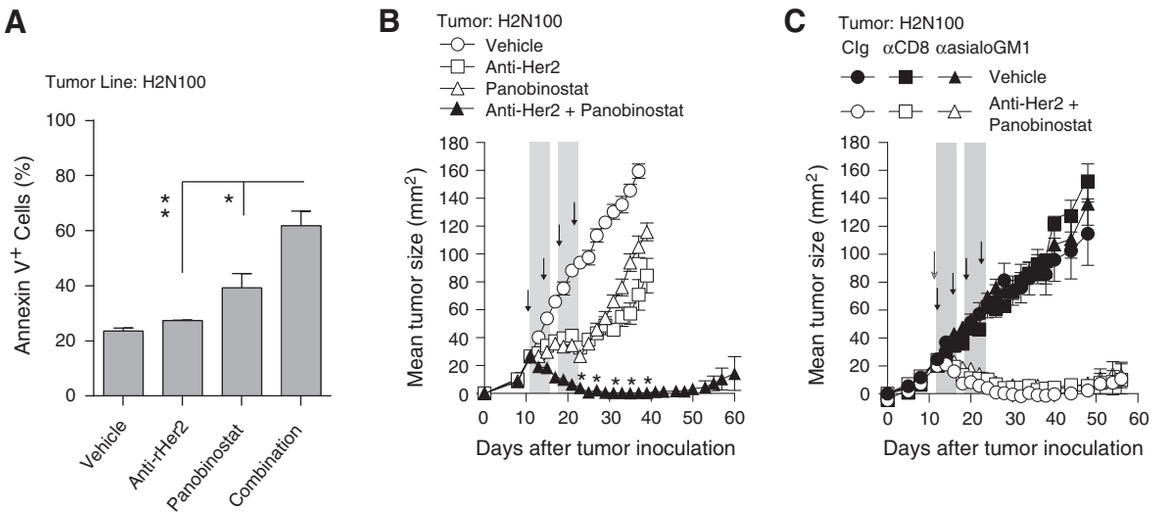

Figure 2.

Cooperative effects of panobinostat and anti-HER2 therapy in syngeneic models of HER2$^+$ mammary cancer. **A,** Sensitivity of the H2N100 tumor line to drug-induced cell death as measured by flow cytometric analysis of Annexin-V staining. Data presented as mean ± SEM of three independent experiments. Statistical differences, *, $P < 0.02$; **, $P < 0.007$. **B** and **C,** HER2/*neu* transgenic mice bearing subcutaneously implanted H2N100 tumors were treated as indicated. Black arrows, treatment with anti-rHER2-therapy (7.16.4). Solid gray bars, periods of HDACi treatment. Gray arrows, start of CIg, α-CD8β or α-asialoGM1 treatment. **B** and **C,** Data presented as mean tumor size ± SEM ($n = 5$–6/group). Results are representative of two-independent experiments. Statistical differences, *, $P < 0.008$ compared with single-agent treatment and control-treated groups.

overcome tumor intrinsic resistance to trastuzumab by engaging host innate immune responses present in SCID but not NSG mice.

Trastuzumab-resistant BT474-MyrAKT tumors are rejected in SCID mice cotreated with panobinostat and trastuzumab

We next sought to derive a trastuzumab-resistant BT474 tumor line. Since oncogene-driven activation of the AKT pathway can confer resistance to trastuzumab (27), we assessed the impact of trastuzumab and panobinostat, alone and in combination on the expression of activated (pAKT) and total AKT protein levels in the BT474 tumors cells. As single agents, both panobinostat and trastuzumab reduced pAKT expression levels (Fig. 4A). Complete ablation of phosphorylated AKT was observed in BT474 cells cotreated with panobinostat and trastuzumab (Fig. 4A). In contrast, no effect of panobinostat and/or trastuzumab on pAKT was observed in the trastuzumab-resistant AU565^{pv} tumor cells (Fig. 4A). Based on these findings, the BT474 tumor line was transduced to express constitutively active myristoylated AKT (MyrAKT), which rendered it insensitive to the cytostatic effects of trastuzumab (Fig. 4B), blocked the dephosphorylation of AKT following exposure to trastuzumab, panobinostat and the combination of both agents (Fig. 4C) and suppressed the combined apoptotic effects of panobinostat and trastuzumab (compare Figs. 1B and 4D).

In NSG mice bearing established BT474-MyrAKT tumors, trastuzumab demonstrated minimal to no effect on tumor growth (Fig. 4E). The anticancer effects of panobinostat were reduced, as was the combined curative activity of panobinostat and trastuzumab (compare Fig. 1C and 4E). These data indicate that constitutive expression of activated AKT was sufficient to protect BT474 tumors from rejection by the combination therapy in NSG mice. Remarkably however in SCID mice, complete regression of established BT474-MyrAKT tumors was evident in all mice cotreated with panobinostat and trastuzumab (Fig. 4E).

NK cells are required to support the combined anticancer activity of panobinostat and anti-HER2 therapy in trastuzumab-resistant HER2$^+$ tumors

We next sought to examine the contribution of innate effector cells to the curative effects of the combination therapy in SCID mice bearing established trastuzumab resistant HER2$^+$ tumors. The therapeutic activity of panobinostat and trastuzumab, alone and in combination, was examined in AU565^{pv} tumor-bearing SCID mice treated with an α-CD11b–targeted antibody that can disrupt the migratory activity of innate immune cells such as NK cells, macrophages and/or neutrophils, all of which express Fc-receptors and can facilitate the cytotoxic actions of trastuzumab (28). Compared with the control immunoglobulin (CIg)–treated mice, α-CD11b treatment completely abrogated the capacity of the combination treatment to eradicate established AU565^{pv} tumors (Fig. 5A). Blockade of the Fc-receptors CD16 (FcγRIII) and CD32 (FcγRII), which are expressed on NK cells (FcγRIII only) and most myeloid cells (29), also reduced the combined curative activity of panobinostat and trastuzumab in AU565^{pv} tumor-bearing SCID mice (Fig. 5B), suggesting that ADCC contributed to the antitumor effects of panobinostat and trastuzumab. Given the reported capacity of NK cells to support the ADCC activity of trastuzumab (30), we examined the combinatorial effects of panobinostat and trastuzumab in AU565^{pv} tumor-bearing SCID mice depleted of NK cells. NK cell depletion abolished the curative activity of the combination therapy (Fig. 5C). We also demonstrated that NK cell reconstitution of NSG mice could significantly enhanced the combined therapeutic

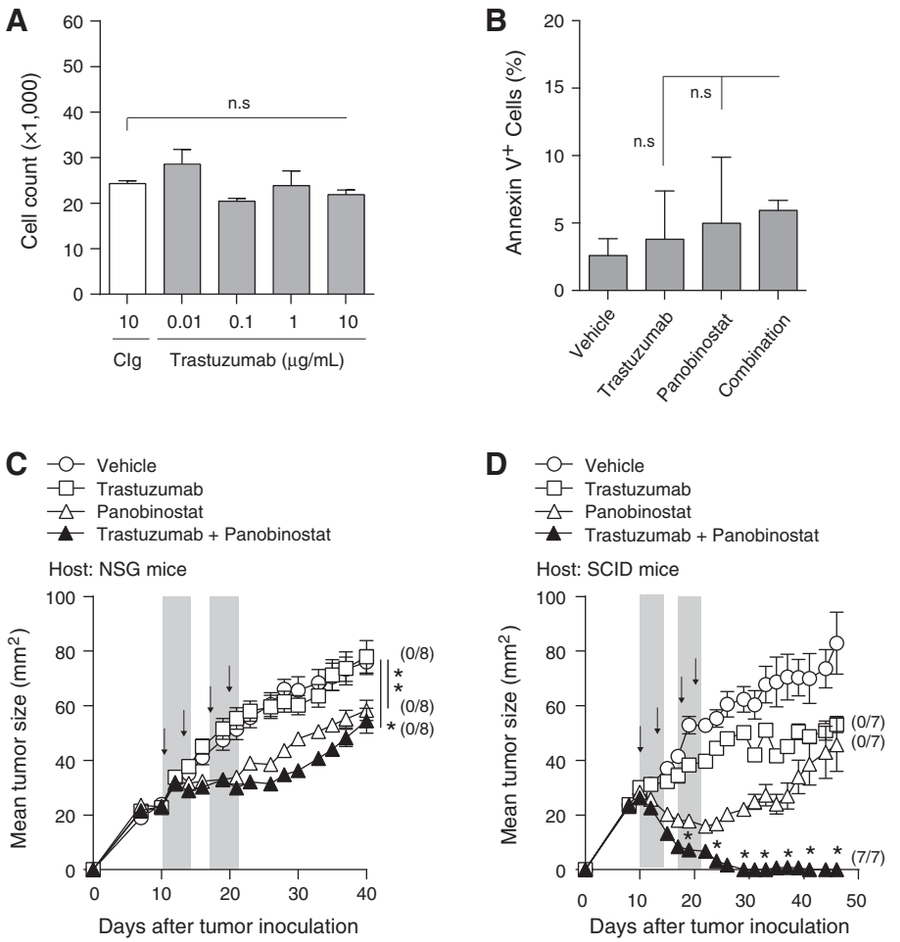

Figure 3.

Host immune defenses support the combined curative activity of panobinostat and trastuzumab against AU565^{pv} tumors. **A,** Antiproliferative effects of trastuzumab on AU565^{pv} tumor cells. **B,** Drug-induced AU565^{pv} tumor cell death as measured by flow cytometric analysis of Annexin-V/PI staining. Mean tumor cell death ± SEM of three-independent experiments shown. **C** and **D,** AU565^{pv} tumor-bearing NSG (**C**) or SCID (**D**) mice were treated as indicated. Black arrows, treatment with trastuzumab. Solid gray bars, periods of HDACi treatment. Mean tumor size ± SEM shown ($n = 7$–8/group). Results are representative of two-independent experiments. Statistical differences, *, $P < 0.008$; **, $P < 0.002$ between the control and combination or panobinostat treatment groups, respectively (**C**); *, $P < 0.008$ compared with single-agent treatment and control-treated groups (**D**). Parentheses indicate the fraction of tumor-free mice.

effects of panobinostat and trastuzumab in AU565^{pv} tumors (Fig. 5D). These studies demonstrate that NK cells are necessary and sufficient to invoke antitumor responses to HER2^{+} trastuzumab-resistant cancers following cotreatment with panobinostat and trastuzumab.

The combined curative response of panobinostat and trastuzumab in AU565^{pv} tumors correlates with an increase in tumor-associated NK cell frequency

Analysis of the immune compartment of AU565^{pv} tumors harvested from *in vivo* therapy experiments revealed that cotreatment with panobinostat and trastuzumab evoked a ≥2-fold increase in tumor-associated CD49b^{+} NK cell frequency, relative to the vehicle and single-agent treatments (Fig. 6A and B). A large proportion of these AU565^{pv}-associated NK cells comprised of CD27^{high}CD11b^{high} and CD27^{low}CD11b^{high} cells (Fig. 6A), which are the most potent NK effector populations (31). The observed increase in tumor-associated NK cell frequency following cotreatment with panobinostat and trastuzumab was evident within one day of treatment initiation, before any detectable therapeutic responses (Fig. 6C). No therapy-induced increases in CD49b^{+} NK cell frequency were observed in the spleens of these mice (Supplementary Fig. S2A and S2B). The administration of antibodies to CD11b, which we previously demonstrated abrogated the curative activity of panobinostat and trastuzumab in AU565^{pv} tumor-bearing SCID mice (Fig. 5A), also selectively restricted therapy-induced NK cell infiltration into the tumors (Fig. 6D); highlighting an important mechanistic link between tumor-associated NK cell frequency and the combined curative activity of panobinostat and trastuzumab.

To characterize the mechanisms by which panobinostat and trastuzumab could collaboratively promote tumor-associated NK cell infiltration, RNA sequencing was performed on whole AU565^{pv} tumors harvested from SCID mice 2 days posttreatment with panobinostat and trastuzumab, alone or in combination. In the trastuzumab-treated AU565^{pv} tumors, no significant changes in immune associated murine gene expression were detected relative to the control-treated tumors (Fig. 7A; GEO accession GSE81380). Panobinostat evoked differential changes in mouse interferon, chemokine and immune response gene signatures that were quantitatively and qualitatively amplified by the concomitant administration of trastuzumab (Fig. 7A, Table 1; GEO accession GSE81380). Most enriched of the gene signatures within the panobinostat + trastuzumab treated AU565^{pv} tumors was the interferon-γ response pathway, which correlated with an increase in expression of the IFNγ response motif STTTCRNTTT_VSIRF_Q6 and STAT1 (GSEA, v2.2.2; Table 1 and Supplementary Fig. S3A). A concomitant increase in mouse CXCL9, CXCL10 and CXCL11 chemokine expression was also

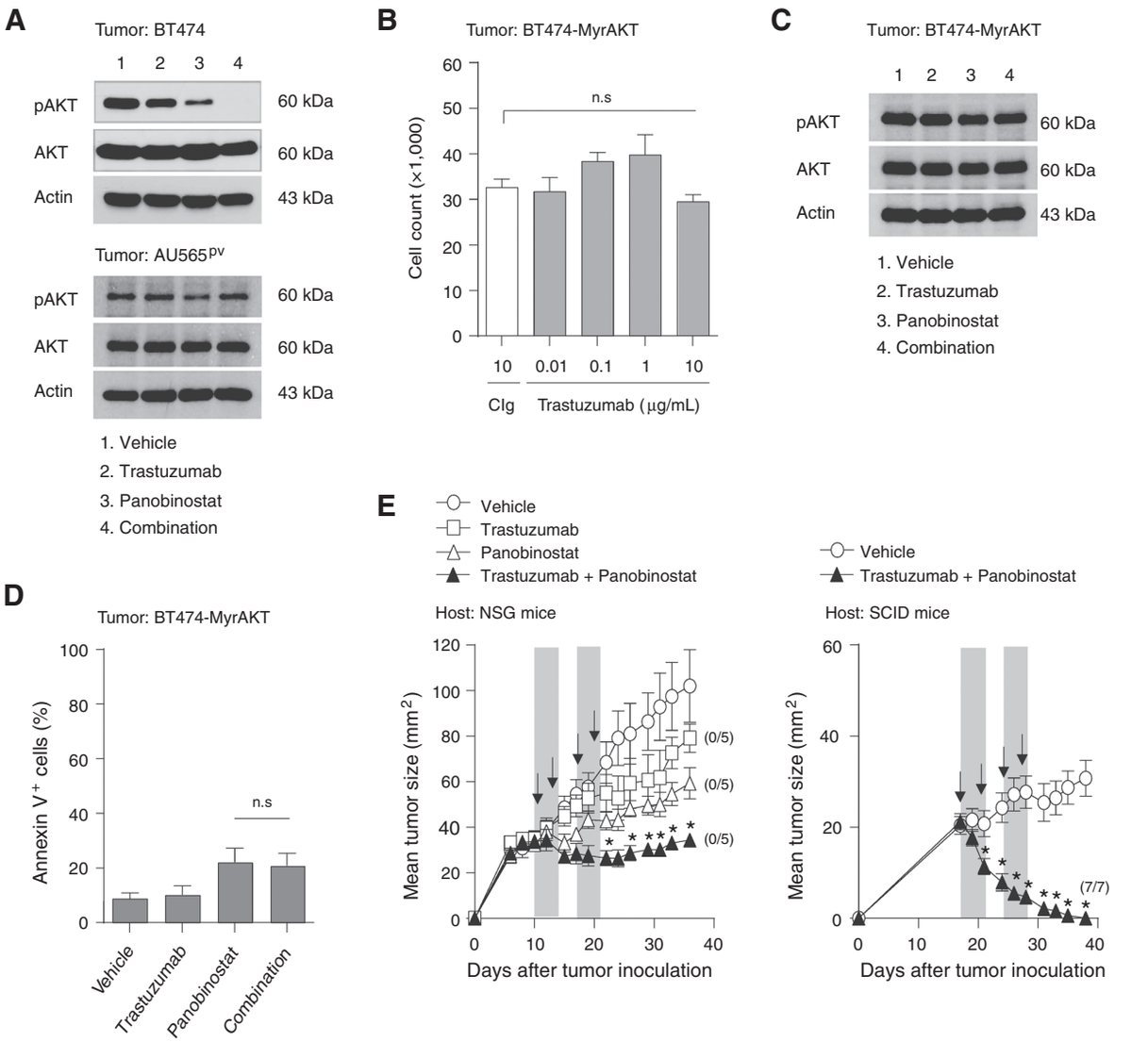

Figure 4.

Trastuzumab-resistant BT474-MyrAKT tumors are rejected in SCID mice cotreated with panobinostat and trastuzumab. **A,** Western blot analysis of pAKT and total AKT protein expression levels in BT474 and AU565^{pv} cells. Data are representative of two-independent experiments. **B,** Antiproliferative effects of trastuzumab on BT474-MyrAKT cells. Mean ± SEM shown ($n = 6$/group); data are representative of two-independent experiments. **C,** Western analysis of pAKT and total AKT protein expression levels in BT474-MyrAKT cells treated as described in **A**. **D,** The percentage of Annexin-V staining was quantitated by flow cytometry. Mean tumor cell death ± SEM of two-independent experiments shown. **E,** BT474-MyrAKT tumor-bearing NSG or SCID mice were treated as indicated. Black arrows, trastuzumab treatment. Gray bars, periods of HDACi treatment. Mean tumor size ± SEM shown ($n = 5$–7/group). Results are representative of two-independent experiments. Statistical differences, *, $P < 0.03$ (**E**; left); *, $P < 0.002$ (**E**; right) compared with the single-agent and control-treated groups. Parentheses indicate the fraction of tumor-free mice.

detected (Supplementary Fig. S3B). These chemokines are ligands for the CXCR3 receptor and are induced by IFNγ–mediated signaling (32). Neutralization of IFNγ significantly abrogated the capacity of the combination therapy to increase NK cell frequency within AU565^{pv} tumors (Fig. 7B). A similar outcome was observed with the concomitant blockade of CXCR3 and Fc-receptors (Fig. 7B). Administration of the CXCR3 or Fc-receptor blocking antibody alone did not affect the ability of the combination therapy to induce a 2-fold increase in NK cell frequency (Fig. 7B). Consistent with these data, IFNγ neutralization or the concomitant blockade of CXCR3 and Fc-receptor signaling in AU565^{pv} tumor-bearing SCID mice significantly inhibited the combined anticancer effects of panobinostat and trastuzumab (Fig. 7C and D). Blockade of CXCR3 signaling alone did not significantly reduce the tumor growth inhibitory effects of the combination therapy (Fig. 7D). A similar outcome was observed with the blockade of CD16/CD32 Fc-receptor signaling in AU565^{pv} tumor bearing SCID mice treated with both panobinostat and trastuzumab, however the long-term curative activity of combination therapy was reduced (Fig. 5B). These data suggest

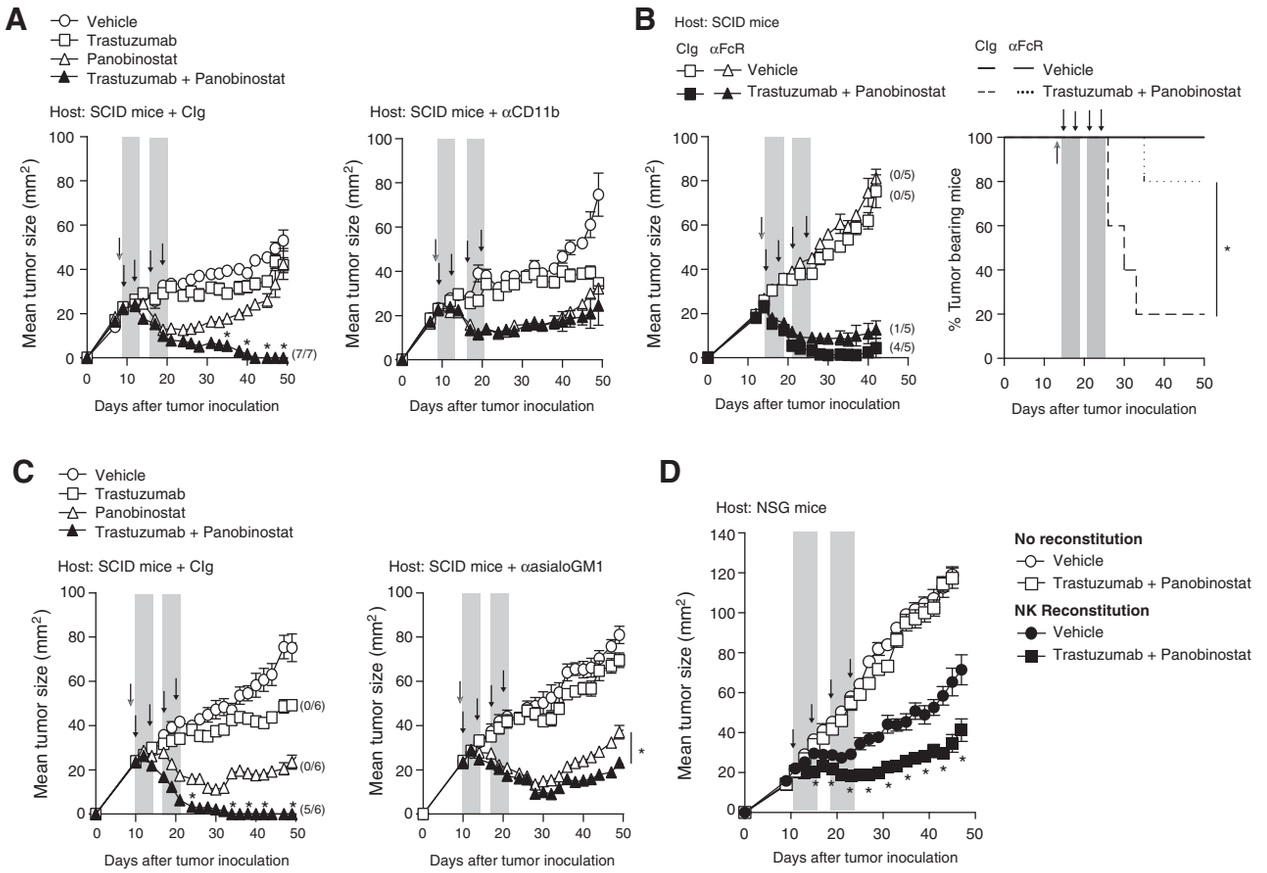

Figure 5.

The combined curative activity of trastuzumab and panobinostat against trastuzumab-resistant HER2$^+$ tumors is dependent on an intact innate immune system. **A–C,** SCID mice bearing established AU565^{pv} tumors were injected with α-CD11b (**A**), α-2.4G2 (**B**), or α-asialoGM1 (**C**) antibodies before the indicated treatments. **D,** AU565^{pv} tumor-bearing NSG mice ± NK cell reconstitution were treated with vehicle or panobinostat + trastuzumab as indicated. **A–D,** Black arrows, treatment with trastuzumab. Gray arrows, start of α-CD11b, α-2.4G2, or α-asialoGM1 treatment. **A–C,** Control mice were treated with Clg. Solid gray bars, periods of HDACi treatment. Mean tumor size ± SEM shown ($n = 5$–7/group). **A** and **C,** Statistical differences, *, $P < 0.008$ compared with single-agent treatment and control-treated groups. **B,** The percentage of tumor-bearing mice following vehicle or combination therapy in the Clg and α-FcR treated groups is shown. Statistical differences, *, $P < 0.002$ between the panobinostat and trastuzumab (combination) ± Clg or α-2.4G2 (α-FcR) treatment groups ($n = 5$/group). **D,** Statistical differences, *, $P < 0.05$ compared with panobinostat + trastuzumab treatment in nonreconstituted AU565^{pv}-tumor bearing NSG mice. Results are representative of one to two independent experiments. Parentheses indicate the fraction of tumor-free mice.

that panobinostat can promote tumor-associated NK cell recruitment and the ADCC activity of trastuzumab by inducing CXCR3-reactive ligand expression locally within the tumor.

Phenotypically, panobinostat treatment promoted expression of the activation marker CD69 and restricted the modulation of Fc-receptor expression on AU565^{pv}-tumor associated NK cells (Supplementary Fig. S4); a phenomenon also observed in IL2-activated mouse and human NK cells treated with panobinostat *in vitro* (Supplementary Fig. S5A and S5B), and supported by the RNA-sequencing analysis of the panobinostat ± trastuzumab treated AU565^{pv} tumors (Supplementary Fig. S3B).

Examination of the *in vitro* cytotoxic activity of IL2-activated mouse NK cells cultured in the presence or absence of panobinostat, revealed that panobinostat could induce a modest improvement in the killing activity of mouse NK cells against treatment naive AU565^{pv} and YAC-1 tumor lines relative to the vehicle-treated NK cells (Supplementary Fig. S5C). Conversely, panobinostat treatment of AU565^{pv} tumor cells did not augment their sensitivity to NK cell killing (Supplementary Fig. S5D). Collective these data suggest that the dominant mechanisms by which panobinostat can enhance trastuzumab-mediated tumor clearance is by promoting tumor-associated NK cell infiltration and effector function.

Discussion

The therapeutic benefit of combining HER2-targeted therapies and HDACi for the treatment of HER2$^+$ cancers has to date largely been examined *in vitro* (11–14). Here, we focused on examining the combined anticancer activity of trastuzumab and panobinostat in models of established HER2$^+$ cancer. Our *in vivo*-based findings highlight the potent ability of panobinostat to augment both the cytostatic and cytotoxic anticancer effects of trastuzumab. In trastuzumab-sensitive HER2$^+$ tumors, tumor intrinsic

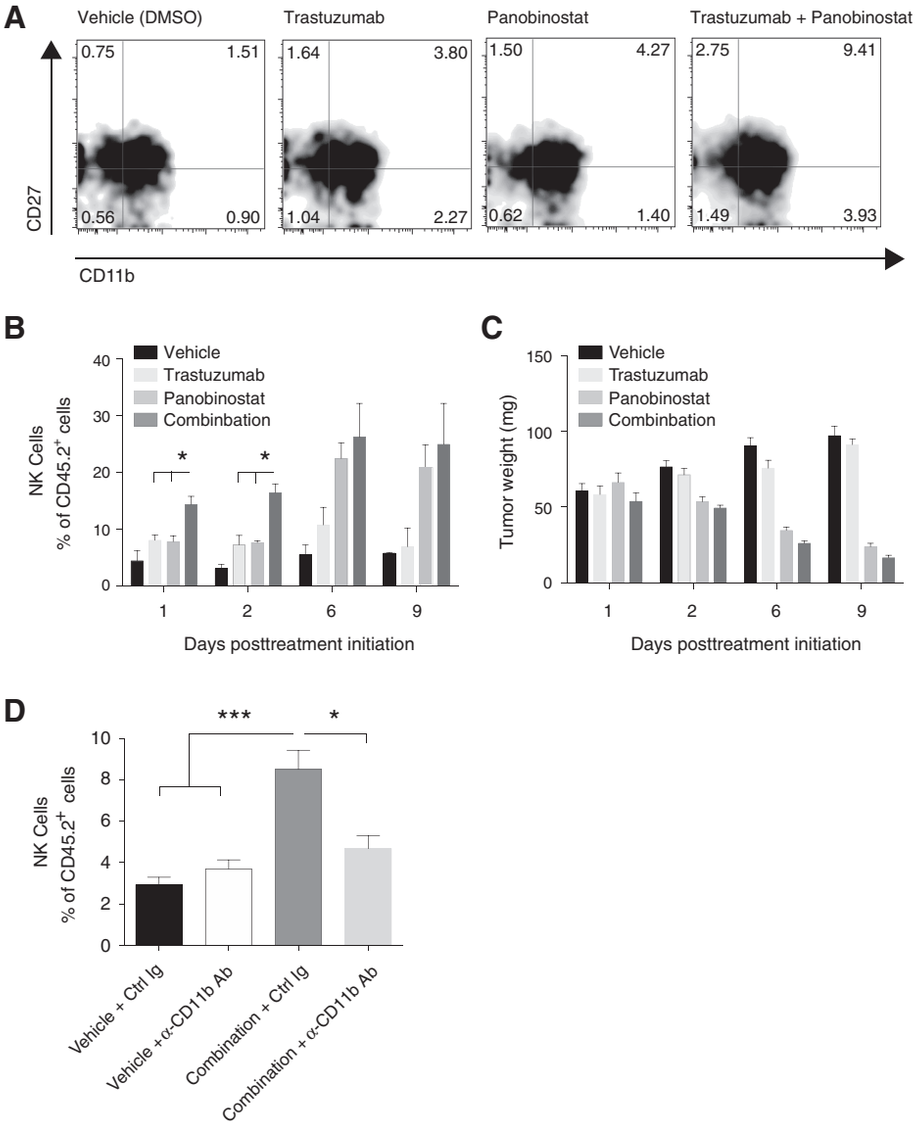

Figure 6.
Cotreatment with panobinostat and trastuzumab induces an increase in AU565^{pv} tumor-associated NK cells. SCID mice bearing AU565^{pv} tumors were treated as indicated. **A,** Flow cytometric analysis on explanted AU565^{pv} tumors. Density plots show levels of CD27 and CD11b expression on AU565^{pv} tumor-infiltrating CD45.2$^+$CD49b$^+$ NK cells (merged data from $n = 4$/group; day 2 posttherapy initiation). Frequency of NK cells in each quadrant is presented as a percentage of the collated viable (DAPI$^-$), CD45.2$^+$ cells. **B,** Frequency of NK cells expressed as a percentage of CD45.2$^+$ cells. Statistical differences, *, $P < 0.05$. **C,** Tumor weight of the explanted AU565^{pv} tumors. Data are presented as mean ± SEM. Results are representative of three independent experiments ($n = 12$/group). **D,** Frequency of CD49b$^+$ NK cells expressed as a percentage of viable (DAPI$^-$), CD45.2$^+$ cells within AU565^{pv} tumors from SCID mice treated with vehicle or panobinostat + trastuzumab (combination) ± CIg or α-CD11b. AU565^{pv} tumors were analyzed day-2 post therapy initiation. Statistical differences, *, $P < 0.01$; ***, $P < 0.001$. Data are presented as mean ± SEM. Results are representative of a single experiment ($n = 7$/group).

mechanisms of cooperation between panobinostat and trastuzumab resulted in the shut-down of AKT signaling, which directly correlated with the curative activity of the combination therapy. The combined ability of panobinostat and trastuzumab to harness host immune effector mechanisms to eradicate HER2$^+$ xenografts was revealed in the setting of trastuzumab-refractory disease. ADCC and IFNγ–mediated, CXCR3-dependent increases in tumor-associated NK cells underpinned the curative activity of the combination therapy in AU565^{pv} xenografts. This is the first study to demonstrate the immune-modulatory potential of this anti–HER2-based combination strategy, and its capacity to eradicate trastuzumab-refractory HER2$^+$ cancer.

The rationale for using panobinostat and trastuzumab in combination for the treatment of HER2$^+$ cancer has been driven by *in vitro* observations demonstrating that HDACi can directly disrupt the HER2-signaling pathway by repressing the *ERBB2* oncogene and/or inactivating PI3K/AKT signaling in tumor cells (33–35). By regulating the chaperone activity of HSP90, following inhibition of HDAC6, panobinostat can alter tumor cell sensitivity to the growth-inhibitory effects of HER2-targeted therapies by promoting the release and degradation of HSP90 client proteins, including HER2 (35, 36) and the subsequent up-regulation of cell-cycle regulatory proteins p21 and p27 (37). In line with this, loss of HER2 was observed in BT474 and BT474-MyrAKT tumor cells cotreated with panobinostat and trastuzumab (Supplementary Fig. S6). Such effects of HDACi and trastuzumab cotreatment on the HER2 signaling pathway have previously been examined *in vitro* (14, 35). In turn, HER2-targeted therapies have been reported to reprogram tumor cell sensitivity to cytotoxic therapy, including HDACi (11, 13) and/or down-regulate tumor cell expression of pro-survival proteins such as Bcl-2 (38). Our *in vivo* analyses of the combined molecular and therapeutic effects of trastuzumab and panobinostat treatment on trastuzumab-sensitive tumors reinforce the collaborative impact of these two anticancer agents on HER2 signaling. Notably, therapy-induced attenuation of pAKT proved to be a reliable biomarker of response to

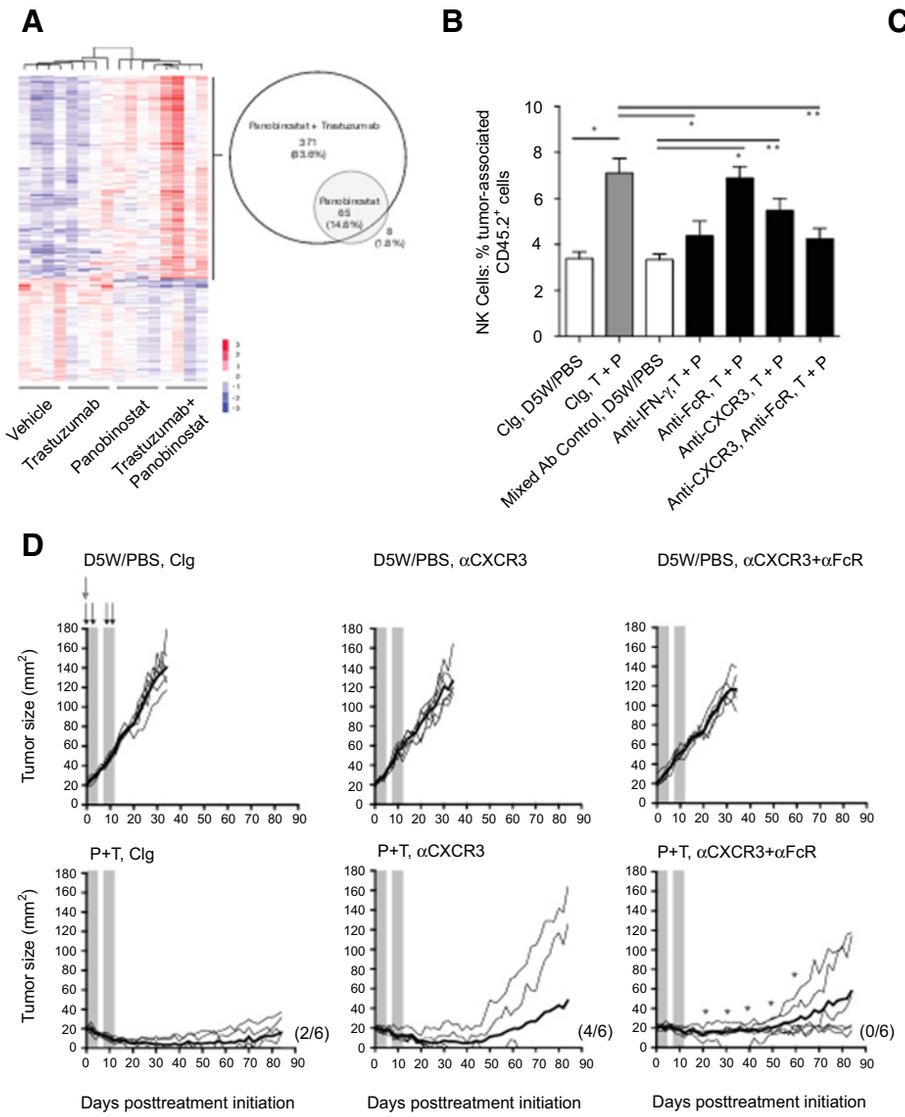

Figure 7.

Cooperative effects of panobinostat and trastuzumab on tumor-associated NK cell recruitment are dependent on IFNγ, CXCR3, and FcR signaling. **A,** RNAseq analysis of whole AU565^{pv} tumors harvested from SCID mice 2-days posttreatment. Heat map shows the differential clustering of genes between each of the treatment groups. Gene set was selected on the basis of normalization of the panobinostat + trastuzumab-treated groups relative to vehicle ($P \leq 0.05$ and a fold-change of $\geq$1). Data were row normalized. Venn diagram shows the relationships that exist between genes upregulated in the panobinostat- ± trastuzumab-treated groups relative to vehicle ($P \leq 0.05$ and a fold-change of $\geq$1). Gene number and frequency of total are shown. **B–D,** SCID mice bearing AU565^{pv} tumors were treated with PBS/DMSO or panobinostat (P) + trastuzumab (T). Antibodies to IFNγ (**B** and **C**), CXCR3 (**B** and **D**), and FcR (CD16/CD32; **B** and **D**) were administered days 0, 1, and every 4 days post therapy initiation. **B,** Flow cytometric analysis was performed on AU565^{pv} tumors 2-days post therapy initiation. Frequency of tumor-associated CD49b$^+$ NK cells is expressed as a percentage of viable (DAPI$^-$), CD45.2$^+$ cells in each of the indicated treatment groups (n = 4–6/group; *, $P < 0.05$; **, $P < 0.008$). Isotype Clg was given in accordance with all other antibody treatments. The mixed Ab control was comprised of all three treatment Abs. **C** and **D,** Gray arrows, the start of Clg, α CXCR3, or α-CXCR3 + α FcR treatment. Black arrows, treatment with trastuzumab. Solid gray bars, periods of HDACi treatment. Data are presented as tumor size (n = 6–7/group). The thin gray lines show tumor growth in each mouse. The solid line shows mean tumor growth for each group. Numbers in parentheses indicate the fraction of tumor-free mice. **C** and **D,** Statistical differences, *, $P < 0.03$ between the α-IFNγ/Clg and α-CXCR3 + α-FcR/Clg, panobinostat + trastuzumab treatment groups.

the curative effects of panobinostat and anti-HER2 therapy in NSG mice. Indeed, the expression of constitutively active AKT (MyrAKT) in BT474 tumor cells was sufficient to render them insensitive to the antiproliferative effects of trastuzumab and rejection by the combination therapy in severely immunocompromised recipient mice. These data, together with the demonstrated efficacy of the combination therapy in immune compromised mice bearing BT474 or H2N100 tumors suggest that tumor-intrinsic mechanisms underpin the collaborative interplay of panobinostat and trastuzumab in HER2$^+$ tumors that are

Table 1. RNA sequencing analysis on whole AU565^{pv} tumors harvested from SCID mice 2 days postinitiation of panobinostat ± trastuzumab treatment

	Panobinostat		Panobinostat + trastuzumab	
Gene set	**NES**	**FDR q-value**	**NES**	**FDR q-value**
IFN_GAMMA_RESPONSE	2.80	<0.00010	2.79	<0.000100
IFN_ALPHA_RESPONSE	2.76	<0.00010	2.67	<0.000100
CHEMOKINE_RECEPTOR BINDING	2.06	0.00125	2.24	<0.000100
CHEMOKINE_ACTIVITY	2.01	0.00341	2.19	<0.000100
IFN response motifs				
STTTCRNTTT_V$IRF_Q6	1.97	0.00640	2.02	0.000968
V$ISRE	1.90	0.00580	1.99	0.000630

NOTE: Therapy-induced, log-fold changes for each treatment group relative to the vehicle (D5W/PBS)-treated AU565^{pv} tumors were examined. The comparative gene sets induced by panobinostat ± trastuzumab are displayed. Normalized enrichment score (NES) and test of statistical significance (FDR *q* value) are shown for each gene set.

inherently sensitive to the cytostatic effects of anti-HER2 therapy. Interestingly doxorubicin failed to augment the efficacy of anti-HER2 therapy when administered intravenously or intratumorally in H2N tumor-bearing syngeneic mice; highlighting the superior therapeutic effects of panobinostat, in the combination setting, over conventional chemotherapy (Supplementary Fig. S7).

The combined potency of the tumor-intrinsic effects of panobinostat and trastuzumab in established BT474 and H2N tumors were likely dominant over any potential immune modulatory effects of the combination therapy. The combined ability of panobinostat and trastuzumab to harness host immune effector mechanisms and clear established disease was revealed in SCID mice bearing trastuzumab-resistant AU565^{pv} and BT474-MyrAKT tumors. Therapy-induced recruitment of NK cells into established AU565^{pv} tumors and promotion of trastuzumab-mediated ADCC was crucial to the curative success of the combination therapy. In line with this, in breast cancer patients, complete and partial therapeutic responses to trastuzumab were documented to correlate with higher *in situ* infiltration of leukocytes and NK/ADCC functions (30, 39). Interestingly in SCID mice, we also demonstrated that Bcl-2 overexpressing AU565^{pv} tumors were susceptible to rejection by the combination therapy (Supplementary Fig. S8), suggesting that the ADCC mechanisms promoted by the combination therapy could bypass key tumor-intrinsic survival pathways that can confer resistance to other conventional breast cancer therapies (40, 41). However, although we have identified an important role for NK cells in supporting the antitumor activity of the combination therapy, we cannot discount the contribution of other Fc-receptor–positive effector cells. Indeed, macrophages express both FcγRII and FcγRIII receptors (29) and can promote NK cell activity via the secretion of pro-inflammatory cytokines and/or direct cell-to-cell contact (28, 42). Interestingly, RNA sequencing of the AU565^{pv} tumors revealed elevated expression levels of the activating Fc receptors FcγRI and FcγRIV (Data not shown; GEO accession GSE81380), the expression of which is associated with monocyte-derived dendritic cells and monocytes/macrophages, respectively (29). Notably, trastuzumab is a humanized IgG1 antibody, the likes of which have been shown to bind all four mouse FcγRs. Human IgG1 antibodies possess similar reactivity against both human and mouse innate effector cells (including NK cells, macrophages and polymorphonuclear leukocytes) and induce potent ADCC in both human and mouse *in vitro* assay systems (43). Compared with human IgG2 and IgG3, IgG1 has proven to be the most potent human isotype in mouse models of cancer, capable of evoking a response profile similar to that of mouse IgG2a, the most potent IgG in mice (43).

By stimulating the local release of IFNγ and CXCR3-reactive chemokines CXCL9, CXCL10 and CXCL11, panobinostat could enhance the cytotoxic functions of trastuzumab by promoting tumor-associated NK cell recruitment. IFNγ is well documented to regulate NK cell frequency and activity within tumors, as well as polarize macrophages toward a tumor-protective M1-state (44). NK cells, particularly the CD27^{high}CD11b^{high} and CD27^{low}CD11b^{high} subpopulations have also been reported to be responsive to CXCR3 ligands (31, 32, 45). By evoking tumor and/or stromal cell death, panobinostat in conjunction with the ADCC functions of trastuzumab may have stimulated a proinflammatory response, leading to the local production of IFNγ and in turn CXCL9, CXCL10, and CXCL11. Panobinostat may have also facilitated the local release of IFNγ by altering the activity of tumor-associated Fc-receptor–positive innate immune cells, through direct epigenetic effects or by promoting the cross communication between these cells (10). Trastuzumab-mediated engagement of Fc-receptors on innate immune cells may have further facilitated the local release of IFNγ (46) as well as stabilized immune cell interactions with the HER2$^+$ tumor cells, a phenomenon that was shown to enhance NKG2D-mediated NK cell cytotoxicity in tumor-bearing syngeneic mice (47). Notably, although the neutralization of IFNγ was sufficient to abrogate the combined effects of panobinostat and trastuzumab on tumor-associate NK cell frequency and AU565^{pv} tumor clearance, the concomitant blockade of both CXCR3 and Fc-receptor signaling was required to achieve a similar outcome; highlighting the collaborative interplay of panobinostat and trastuzumab in evoking the eradication of HER2$^+$ tumors that are refractory to the cytostatic effects of trastuzumab.

Given the pleiotropic antitumor responses elicited by HDACi, as well as the manageable toxicity profile for these agents (48, 49) we predict that panobinostat could greatly complement standard chemotherapy care and enhance the treatment of HER2$^+$ breast tumors when combined with trastuzumab. Ultimately, the proven collaborative efficacy of panobinostat and trastuzumab in established HER2$^+$ breast tumors, whether molecularly sensitive or resistant to trastuzumab therapy, provides strong rationale for pursuing the clinical development of this anti-HER2-based combination strategy.

Disclosure of Potential Conflicts of Interest

R.W. Johnstone reports receiving a commercial research grant from Novartis and AstraZeneca, and has received speakers bureau honoraria from Novartis. No potential conflicts of interest were disclosed by the other authors.

Authors' Contributions

Conception and design: M. Medon, J.A. Trapani, P.W. Atadja, M.A. Henderson, R.W. Johnstone, N.M. Haynes
Development of methodology: M. Medon, N.M. Haynes
Acquisition of data (provided animals, acquired and managed patients, provided facilities, etc.): M. Medon, E. Vidacs, M.R. Jenkins, K.M. Ramsbottom, M.J. Smyth, M.A. Henderson, N.M. Haynes
Analysis and interpretation of data (e.g., statistical analysis, biostatistics, computational analysis): M. Medon, S.J Vervoort, J. Li, M.R. Jenkins, P.K Darcy, P.W. Atadja, M.A. Henderson, N.M. Haynes
Writing, review, and/or revision of the manuscript: M. Medon, J. Li, J.A. Trapani, M.J. Smyth, P.K Darcy, P.W. Atadja, M.A. Henderson, R.W. Johnstone, N.M. Haynes
Administrative, technical, or material support (i.e., reporting or organizing data, constructing databases): M. Medon, E. Vidacs, J. Li, M.A. Henderson, N.M. Haynes
Study supervision: P.W. Atadja, M.A. Henderson, R.W. Johnstone, N.M. Haynes
Other (performed animal work and procedures on the animals): E. Vidacs,

Acknowledgments

The authors thank Associate Prof. B. Chua for her intellectual input into the project, S.J. Haikerwal for technical assistance with the tissue analysis work, Dr. P. Beavis for his assistance with the preparation of the tumor samples for RNA sequencing, Dr. P. Neeson for provision of anti-human antibodies for the study of NK ligand expression on human breast cancer lines, Dr. C. Kearney for the provision of IL2-activated mouse NK cells, Dr. R. Pearson for provision of the MK-2206 inhibitor and K. Papastratos, S. Brown, and E. McGuire for technical assistance with the animal husbandry work.

Grant Support

This work was financially supported by Victorian Breast Cancer Research Consortium (R.W. Johnstone, M. Medon, and N.M. Haynes); National Health and Medical Research Council of Australia (NHMRC) and Victorian Cancer Agency (R.W Johnstone); Cancer Council of Victoria (N.M. Haynes and R.W. Johnstone).

The costs of publication of this article were defrayed in part by the payment of page charges. This article must therefore be hereby marked *advertisement* in accordance with 18 U.S.C. Section 1734 solely to indicate this fact.

Received August 18, 2016; revised October 4, 2016; accepted February 27, 2017; published OnlineFirst March 1, 2017.

References

1. Slamon DJ, Godolphin W, Jones LA, Holt JA, Wong SG, Keith DE, et al. Studies of the HER-2/neu proto-oncogene in human breast and ovarian cancer. Science 1989;244:707–12.
2. Harari D, Yarden Y. Molecular mechanisms underlying ErbB2/HER2 action in breast cancer. Oncogene 2000;19:6102–14.
3. Recondo G, Diaz Canton E, de la Vega M, Greco M, Recondo G, Valsecchi ME. Therapeutic options for HER-2 positive breast cancer: Perspectives and future directions. World J Clin Oncol 2014;5:440–54.
4. Bianchini G, Gianni L. The immune system and response to HER2-targeted treatment in breast cancer. Lancet Oncol 2014;15:e58–68.
5. Tinoco G, Warsch S, Gluck S, Avancha K, Montero AJ. Treating breast cancer in the 21st century: emerging biological therapies. J Cancer 2013;4:117–32.
6. West AC, Johnstone RW. New and emerging HDAC inhibitors for cancer treatment. J Clin Invest 2014;124:30–9.
7. Bridle BW, Chen L, Lemay CG, Diallo JS, Pol J, Nguyen A, et al. HDAC inhibition suppresses primary immune responses, enhances secondary immune responses, and abrogates autoimmunity during tumor immunotherapy. Mol Ther 2013;21:887–94.
8. Christiansen AJ, West A, Banks KM, Haynes NM, Teng MW, Smyth MJ, et al. Eradication of solid tumors using histone deacetylase inhibitors combined with immune-stimulating antibodies. Proc Natl Acad Sci U S A 2011;108:4141–6.
9. Zhang F, Zhou X, DiSpirito JR, Wang C, Wang Y, Shen H. Epigenetic manipulation restores functions of defective CD8(+) T cells from chronic viral infection. Mol Ther 2014;22:1698–706.
10. Kroesen M, Gielen P, Brok IC, Armandari I, Hoogerbrugge PM, Adema GJ. HDAC inhibitors and immunotherapy; a double edged sword? Oncotarget 2014;5:6558–72.
11. Bali P, Pranpat M, Swaby R, Fiskus W, Yamaguchi H, Balasis M, et al. Activity of suberoylanilide hydroxamic acid against human breast cancer cells with amplification of Her-2. Clin Cancer Res 2005;11:6382–9.
12. LaBonte MJ, Wilson PM, Fazzone W, Russell J, Louie SG, El-Khoueiry A, et al. The dual EGFR/HER2 inhibitor lapatinib synergistically enhances the antitumor activity of the histone deacetylase inhibitor panobinostat in colorectal cancer models. Cancer Res 2011;71:3635–48.
13. Huang X, Wang S, Lee CK, Yang X, Liu B. HDAC inhibitor SNDX-275 enhances efficacy of trastuzumab in erbB2-overexpressing breast cancer cells and exhibits potential to overcome trastuzumab resistance. Cancer Lett 2011;307:72–9.
14. Fuino L, Bali P, Wittmann S, Donapaty S, Guo F, Yamaguchi H, et al. Histone deacetylase inhibitor LAQ824 down-regulates Her-2 and sensitizes human breast cancer cells to trastuzumab, taxotere, gemcitabine, and epothilone B. Mol Cancer Ther 2003;2:971–84.
15. Tu Y, Hershman DL, Bhalla K, Fiskus W, Pellegrino CM, Andreopoulou E, et al. A phase I-II study of the histone deacetylase inhibitor vorinostat plus sequential weekly paclitaxel and doxorubicin-cyclophosphamide in locally advanced breast cancer. Breast Cancer Res Treat 2014;146:145–52.
16. Lustberg MB, Ramaswamy B. Epigenetic therapy in breast cancer. Curr Breast Cancer Rep 2011;3:34–43.
17. Di Carlo E, Diodoro MG, Boggio K, Modesti A, Modesti M, Nanni P, et al. Analysis of mammary carcinoma onset and progression in HER-2/neu oncogene transgenic mice reveals a lobular origin. Lab Invest 1999;79:1261–9.
18. Lindemann RK, Newbold A, Whitecross KF, Cluse LA, Frew AJ, Ellis L, et al. Analysis of the apoptotic and therapeutic activities of histone deacetylase inhibitors by using a mouse model of B cell lymphoma. Proc Natl Acad Sci U S A 2007;104:8071–6.
19. Shortt J, Martin BP, Newbold A, Hannan KM, Devlin JR, Baker AJ, et al. Combined inhibition of PI3K-related DNA damage response kinases and mTORC1 induces apoptosis in MYC-driven B-cell lymphomas. Blood 2013;121:2964–74.
20. Wendel HG, De Stanchina E, Fridman JS, Malina A, Ray S, Kogan S, et al. Survival signalling by Akt and eIF4E in oncogenesis and cancer therapy. Nature 2004;428:332–7.
21. Stagg J, Sharkey J, Pommey S, Young R, Takeda K, Yagita H, et al. Antibodies targeted to TRAIL receptor-2 and ErbB-2 synergize in vivo and induce an antitumor immune response. Proc Natl Acad Sci U S A 2008;105:16254–9.
22. Haynes NM, Hawkins ED, Li M, McLaughlin NM, Hammerling GJ, Schwendener R, et al. CD11c+ dendritic cells and B cells contribute to the tumoricidal activity of anti-DR5 antibody therapy in established tumors. J Immunol 2010;185:532–41.
23. Kim D, Pertea G, Trapnell C, Pimentel H, Kelley R, Salzberg SL. TopHat2: accurate alignment of transcriptomes in the presence of insertions, deletions and gene fusions. Genome Biol 2013;14:R36.
24. Anders S, Pyl PT, Huber W. HTSeq–a Python framework to work with high-throughput sequencing data. Bioinformatics 2015;31:166–9.
25. Law CW, Chen Y, Shi W, Smyth GK. voom: Precision weights unlock linear model analysis tools for RNA-seq read counts. Genome Biol 2014;15:R29.
26. Shultz LD, Schweitzer PA, Christianson SW, Gott B, Schweitzer IB, Tennent B, et al. Multiple defects in innate and adaptive immunologic function in NOD/LtSz-scid mice. J Immunol 1995;154:180–91.
27. O'Brien NA, Browne BC, Chow L, Wang Y, Ginther C, Arboleda J, et al. Activated phosphoinositide 3-kinase/AKT signaling confers resistance to trastuzumab but not lapatinib. Mol Cancer Ther 2010;9:1489–502.
28. Clynes RA, Towers TL, Presta LG, Ravetch JV. Inhibitory Fc receptors modulate in vivo cytotoxicity against tumor targets. Nat Med 2000;6:443–6.

29. Bruhns P. Properties of mouse and human IgG receptors and their contribution to disease models. Blood 2012;119:5640–9.
30. Beano A, Signorino E, Evangelista A, Brusa D, Mistrangelo M, Polimeni MA, et al. Correlation between NK function and response to trastuzumab in metastatic breast cancer patients. J Transl Med 2008;6:25.
31. Hayakawa Y, Smyth MJ. CD27 dissects mature NK cells into two subsets with distinct responsiveness and migratory capacity. J Immunol 2006; 176:1517–24.
32. Van Raemdonck K, Van den Steen PE, Liekens S, Van Damme J, Struyf S. CXCR3 ligands in disease and therapy. Cytokine Growth Factor Rev 2015;26:311–27.
33. Kim YJ, Greer CB, Cecchini KR, Harris LN, Tuck DP, Kim TH. HDAC inhibitors induce transcriptional repression of high copy number genes in breast cancer through elongation blockade. Oncogene 2013;32:2828–35.
34. Wilson-Edell KA, Yevtushenko MA, Rothschild DE, Rogers AN, Benz CC. mTORC1/C2 and pan-HDAC inhibitors synergistically impair breast cancer growth by convergent AKT and polysome inhibiting mechanisms. Breast Cancer Res Treat 2014;144:287–98.
35. Bali P, Pranpat M, Bradner J, Balasis M, Fiskus W, Guo F, et al. Inhibition of histone deacetylase 6 acetylates and disrupts the chaperone function of heat shock protein 90: a novel basis for antileukemia activity of histone deacetylase inhibitors. J Biol Chem 2005;280:26729–34.
36. Citri A, Kochupurakkal BS, Yarden Y. The achilles heel of ErbB-2/HER2: regulation by the Hsp90 chaperone machine and potential for pharmacological intervention. Cell Cycle 2004;3:51–60.
37. Newbold A, Salmon JM, Martin BP, Stanley K, Johnstone RW. The role of p21 and p27 in HDACi-mediated tumor cell death and cell cycle arrest in the Emu-myc model of B-cell lymphoma. Oncogene 2014;33:5415–23.
38. Milella M, Trisciuoglio D, Bruno T, Ciuffreda L, Mottolese M, Cianciulli A, et al. Trastuzumab down-regulates Bcl-2 expression and potentiates apoptosis induction by Bcl-2/Bcl-XL bispecific antisense oligonucleotides in HER-2 gene–amplified breast cancer cells. Clin Cancer Res 2004;10:7747–56.
39. Varchetta S, Gibelli N, Oliviero B, Nardini E, Gennari R, Gatti G, et al. Elements related to heterogeneity of antibody-dependent cell cytotoxicity in patients under trastuzumab therapy for primary operable breast cancer overexpressing Her2. Cancer Res 2007;67:11991–9.
40. Oakes SR, Vaillant F, Lim E, Lee L, Breslin K, Feleppa F, et al. Sensitization of BCL-2-expressing breast tumors to chemotherapy by the BH3 mimetic ABT-737. Proc Natl Acad Sci U S A 2012;109:2766–71.
41. Simoes-Wust AP, Schurpf T, Hall J, Stahel RA, Zangemeister-Wittke U. Bcl-2/bcl-xL bispecific antisense treatment sensitizes breast carcinoma cells to doxorubicin, paclitaxel and cyclophosphamide. Breast Cancer Res Treat 2002;76:157–66.
42. Michel T, Hentges F, Zimmer J. Consequences of the crosstalk between monocytes/macrophages and natural killer cells. Front Immunol 2012; 3:403.
43. Overdijk MB, Verploegen S, Ortiz Buijsse A, Vink T, Leusen JH, Bleeker WK, et al. Crosstalk between human IgG isotypes and murine effector cells. J Immunol 2012;189:3430–8.
44. Marcus A, Gowen BG, Thompson TW, Iannello A, Ardolino M, Deng W, et al. Recognition of tumors by the innate immune system and natural killer cells. Adv Immunol 2014;122:91–128.
45. Wennerberg E, Kremer V, Childs R, Lundqvist A. CXCL10-induced migration of adoptively transferred human natural killer cells toward solid tumors causes regression of tumor growth in vivo. Cancer Immunol Immunother 2015;64:225–35.
46. Shi Y, Fan X, Meng W, Deng H, Zhang N, An Z. Engagement of immune effector cells by trastuzumab induces HER2/ERBB2 downregulation in cancer cells through STAT1 activation. Breast Cancer Res 2014;16:R33.
47. Deguine J, Breart B, Lemaitre F, Bousso P. Cutting edge: tumor-targeting antibodies enhance NKG2D-mediated NK cell cytotoxicity by stabilizing NK cell-tumor cell interactions. J Immunol 2012;189:5493–7.
48. San-Miguel JF, Richardson PG, Gunther A, Sezer O, Siegel D, Blade J, et al. Phase Ib study of panobinostat and bortezomib in relapsed or relapsed and refractory multiple myeloma. J Clin Oncol 2013;31:3696–703.
49. Richardson PG, Schlossman RL, Alsina M, Weber DM, Coutre SE, Gasparetto C, et al. PANORAMA 2: panobinostat in combination with bortezomib and dexamethasone in patients with relapsed and bortezomib-refractory myeloma. Blood 2013;122:2331–7.